Intraprotein Electron Transfer in a Two-Domain Construct of Neuronal Nitric Oxide Synthase: The Output State in Nitric Oxide Formation†

Changjian Feng,*,‡ Gordon Tollin,*,§ Michael A. Holliday,|| Clayton Thomas,|| John C. Salerno,⊥ John H. Enemark,# and Dipak K. Ghosh*,||

College of Pharmacy, University of New Mexico, Albuquerque, New Mexico 87131, Department of Biochemistry and Molecular Biophysics, University of Arizona, Tucson, Arizona 85721, Department of Medicine, Duke University and VA Medical Centers, Durham, North Carolina 27705, Department of Biology, Rensselaer Polytechnic Institute, Troy, New York 1485, and Department of Chemistry, University of Arizona, Tucson, Arizona 85721

Received February 2, 2006; Revised Manuscript Received March 28, 2006

ABSTRACT: Intersubunit intraprotein electron transfer (IET) from flavin mononucleotide (FMN) to heme is essential in nitric oxide (NO) synthesis by NO synthase (NOS). Previous crystal structures and functional studies primarily concerned an enzyme conformation, which serves as the input state for reduction of FMN by electrons from NADPH and flavin adenine dinucleotide (FAD) in the reductase domain. To favor the formation of the output state for the subsequent IET from FMN to heme in the oxygenase domain, a novel truncated two-domain oxyFMN construct of rat neuronal NOS (nNOS), in which only the FMN and heme domains were present, was designed and expressed. The kinetics of IET between the FMN and heme domains in the nNOS oxyFMN construct in the presence and absence of added calmodulin (CaM) were directly determined using laser flash photolysis of CO dissociation in comparative studies on partially reduced oxyFMN and single-domain heme oxygenase constructs. The IET rate constant in the presence of CaM (262 s^{-1}) was increased approximately 10-fold compared to that in the absence of CaM (22 s^{-1}). The effect of CaM on interdomain interactions was further evidenced by electron paramagnetic resonance (EPR) spectra. This work provides the first direct evidence of the CaM control of electron transfer (ET) between FMN and heme domains through facilitation of the FMN/heme interactions in the output state. Therefore, CaM controls IET between heme and FMN domains by a conformational gated mechanism. This is essential in coupling ET in the reductase domain in NOS with NO synthesis in the oxygenase domain.

Nitric oxide (NO), a ubiquitous cellular signaling molecule, is one of the most studied small molecules in biology because of its involvement in numerous biological events such as vasodilation, neurotransmission, and immune response (*1*). In mammals, NO is synthesized by nitric oxide synthase (NOS),[1] a homodimeric flavo-hemoprotein that catalyzes the 5-electron oxidation of L-arginine (Arg) to NO and L-citrulline with NADPH and O_2 as cosubstrates (*2*). There are three mammalian NOS isoforms: endothelial (eNOS), neuronal (nNOS), and inducible (iNOS). Each chain of all three isoforms contains a C-terminal electron-supplying reductase unit with binding sites for NADPH (electron source), flavin adenine dinucleotide (FAD), and flavin mononucleotide (FMN) and an N-terminal catalytic heme-containing oxygenase domain; these components are linked by a calmodulin (CaM) binding region. The substrate, L-arginine, and a cofactor, (6R)-5,6,7,8-tetrahydrobiopterin (H_4B), both bind near the heme center in the oxygenase domain (*3*). The structure of the holoenzyme is not yet available, although extensive crystallographic studies of the oxygenase domain have been performed (*4*−*7*). Only a few crystal structures of nNOS reductase domains (*8*, *9*) and homologues (*10*) have been reported, and these have provided new insights into the function of these enzymes.

A unique feature of nNOS and eNOS is that CaM binding facilitates efficient intersubunit intramolecular electron transfer (IET) from NADPH to heme, leading to NO synthesis at the oxygenase active site (*11*, *12*). The effect of CaM in controlling IET in NOS can be indirectly probed by the kinetics of CO binding (*13*), NO production (*14*), NADPH consumption (*11*), or cytochrome *c* reduction (*11*).

The major difference between the CaM-regulated isoforms eNOS and nNOS and the inducible isoform iNOS, which binds CaM at all physiological Ca^{2+} concentrations, is the presence of internal control elements (*11*, *15*). Identified

† This work was supported by Grant AHA 0365338U to D.K.G. from the American Heart Association.

* To whom correspondence should be addressed. E-mail: cfeng@salud.unm.edu. Telephone: 505-925-4326. Fax: 505-272-6749 (C.F.); E-mail: gtollin@u.arizona.edu. Fax: 520-621-9288 (G.T.); E-mail: dgx@acpub.duke.edu. Telephone: 919-286-0411 ext. 15249. Fax: 919-286-6891 (D.K.G.).

‡ University of New Mexico.

§ Department of Biochemistry and Molecular Biophysics, University of Arizona.

|| Duke University and VA Medical Centers.

⊥ Rensselaer Polytechnic Institute.

Department of Chemistry, University of Arizona.

[1] Abbreviations: NOS, nitric oxide synthase; nNOS, neuronal NOS; CaM, calmodulin; oxyFMN, two-domain NOS construct in which only FMN and heme domains are present; nNOSoxy, nNOS oxygenase construct; IET, intramolecular electron transfer; dRF and dRFH·, 5-deazariboflavin and 5-deazariboflavin semiquinone, respectively.

10.1021/bi060223n CCC: $33.50
Published on Web 04/27/2006

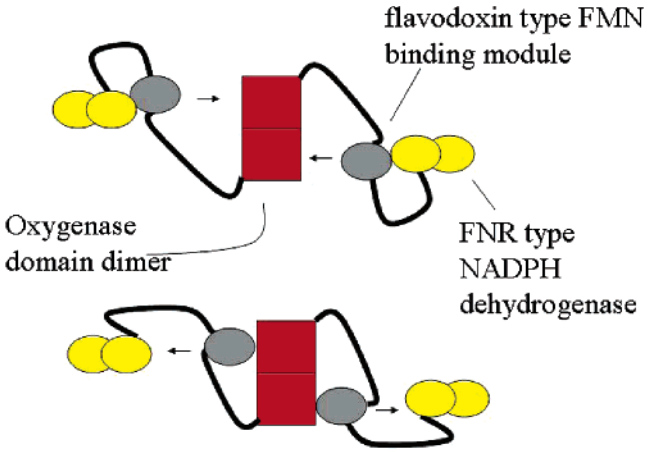

FIGURE 1: Tethered shuttle model. Flavodoxin-type FMN-binding domain (gray) shuttles between the flavodoxin−NADPH reductase (FNR)-type two-domain "dehydrogenase unit" (yellow) and the oxygenase domain dimer (red). (Top) Putative input state. (Bottom) Putative output state.

originally from sequence alignments and modeling and postulated to restrict alignment of the FMN-binding domain with the oxygenase and/or FAD-binding domains (*15*), the FMN domain autoinhibitory element pins the FMN-binding domain to the reductase complex via a network of hydrogen bonds (*8*).

Although many details of the NOS mechanism remain to be elucidated, it is well-established that IET processes are key steps in the regulation of NO synthesis (*16*, *17*). It is thus of significant interest to investigate the thermodynamics (*18*−*20*) and kinetics (*13*, *14*, *21*) of electron transfer (ET). A major obstacle in kinetics studies is that the absorption spectra of the FAD and FMN moieties in the holoenzyme are nearly identical, making direct observation of discrete ET steps involving these two cofactors difficult.

Recent crystallographic studies of the NOS reductase unit (*8*) and of the homologous NADPH P450 reductase (*10*) have revealed a structure in which the flavodoxin-like FMN-binding domain is tightly associated with the flavodoxin−NADPH reductase-like two-domain C-terminal unit, forming a complex in which electrons can readily pass from NADPH to FAD via a charge-transfer intermediate and hence to the FMN isoalloxazine system, located within 5 Å of the FAD isoalloxazine in an edge-on configuration. However, in this complex, the FMN is inaccessible to electron acceptors, including the heme of the oxygenase domain. It has been proposed that the oxygenase heme could not be docked within 25 Å of the FMN in the original P450 reductase structure (*22*). Furthermore, the ancestral ET systems (e.g., flavodoxin/flavodoxin reductase) operate with flavodoxin as a shuttle between the two-domain reductase and other components such as photosystem I (Figure 1). It is likely that in modular enzymes containing domains derived from these ancestors a tethered shuttle still operates, with the tethers corresponding to the FMN−oxygenase and FAD−FMN connectors in NOS. The tethered shuttle model involves an input state corresponding to the existing reductase structures and an output state in which the FMN-binding domain associates with the oxygenase domain.

To observe the output state of the shuttle mechanism, we designed a series of novel two-domain NOS oxyFMN constructs in which only the FMN and oxygenase domains along with the CaM binding sequence are expressed to favor the interaction of the FMN-binding domain with the oxygenase domain over interactions within the reductase unit (*23*). The absence of FAD in this construct facilitates the direct observation of discrete ET between FMN and heme in nNOS without interference by FAD. More importantly, the absence of the two-domain "NADPH dehydrogenase" unit removes the dominant input-state complex from the conformational repertoire of the construct. This provides us with a greatly enhanced opportunity to observe the putative output state, in which the FMN-binding site is closely associated with the oxygenase active site rather than with the dehydrogenase active site.

In this work, as part of a systematic study of IET in the catalytic cycle of NOS, we have used laser flash photolysis of CO dissociation in comparative studies on partially reduced rat nNOS oxyFMN and single-domain heme oxygenase (nNOSoxy) constructs to *directly* observe the kinetics of the IET between the FMN and heme domains in the two-domain construct. In addition, we have demonstrated an essential role of CaM in the activation of IET between these two domains by directly following this step.

EXPERIMENTAL PROCEDURES

Cloning and Protein Purification. The NOS oxyFMN construct consists of residues 291−947; the short C-terminal sequence was included because it is closely associated with the FMN-binding domain, and the N-terminal truncation removes the PDZ domain, which functions as a protein interaction site in nNOS. The N-terminal portion of the construct thus corresponds closely to nNOS oxygenase domains, which have been successfully crystallized, and includes the Zn^{2+}-binding site present in eukaryotic but not prokaryotic NOS sequences.

A Clonetech high-fidelity polymerase chain reaction (PCR) kit was employed for cloning of the nNOS oxyFMN construct. Using rat nNOS as a template, PCR was used to amplify cDNA encoding residues 291−947 (for rat nNOS) to add a sequence coding for a His_6 tag at the N-terminal end of the protein. PCR products were subcloned into the *Escherichia coli* expression vector pCWori+ (*23*). Delta 290 rat nNOSoxy (residues 291−722 in rat nNOS oxygenase domain) was expressed and purified as reported earlier (*23*) and previously for the NOS oxygenase domain (*4*, *24*). The pCWori+ vector expressing rat nNOS oxyFMN was transformed into a protease-deficient *E. coli* strain BL21DE3 (Novagen, Madison, WI) as described for the oxygenase domain (*23*). Cells were grown in Terrific Broth (Sigma) containing 125 μg/mL ampicillin. Cultures were shaken at 250 rpm at 37 °C until an OD of 1.0 at 600 nm was reached. Protein expression was induced by adding 0.5 mM isopropyl-β-D-thiogalactopyranoside (IPTG) plus 0.4 mM of the heme precursor δ-aminolevulinic acid, and shaking was continued for 42 h at 22 °C (*24*). Cell harvest and subsequent protein purification through Ni^{2+}-NTA Sepharose 4B metal chelate affinity resin (Novagen, Madison, WI) and CaM Sepharose affinity column (Amersham Bioscience, Piscataway, NJ) were done in the same way with a slight modification of our earlier procedure (*23*), where rat brain CaM (Sigma, St. Louis, MO) was added at a ~2 μM concentration during the lysate preparation to protect the CaM-binding site during

cell lysis and processing. The added CaM was not co-purified with nNOS oxyFMN during column purification. The H_4B content in the protein was 4 μM, and the exogenous concentrations of H_4B and FMN present in the final stage of purification were 4 and 2 μM, respectively (*23*).

UV−Vis Spectra of the nNOS oxyFMN Construct in the Reduction/Oxidation Cycle. UV−vis spectrum of the nNOS oxyFMN construct was observed at 1, 2, or 5 μM in 50 mM 3-(*N*-morpholino)propanesulfonic acid (MOPS) in the presence of 5% glycerol with an Olis converted Aminco DW200 spectrophotometer. Experiments were performed in a stoppered cuvette under argon. After nNOS oxyFMN was reduced with small volumes of buffered dithionite solution until the 480 and 650 nm bands were bleached, the introduction of about 300 mL of air caused reoxidation of the protein to a state in which heme was oxidized but FMN was in the blue neutral semiquinone.

Electron Paramagnetic Resonance (EPR) Spectroscopy. EPR spectra were recorded on a Bruker EPR spectrometer with a flowing helium cryostat as previously described (*25*). Samples were frozen quickly and stored in liquid nitrogen.

Laser Flash Photolysis. A deazariboflavin (dRF) solution in pH 7.6 buffer (40 mM Bis-Tris propane, 400 mM NaCl, 2 mM L-arginine, 1 mM Ca^{2+}, and 10% glycerol) was well-degassed by a mixture of Ar and CO (with a ratio of ~2:1). L-Arginine was added to keep oxidized heme in a high-spin state, and Ca^{2+} was present in all of the experiments involving the subsequent addition of CaM. Aliquots of concentrated protein were subsequently injected, and the solution was further purged with the Ar/CO mixture to remove any added oxygen before being subjected to laser flash photolysis. The oxidized protein solution in the presence of dRF was flashed by 400 nm laser excitation to follow reactions between the protein and 5-deazariboflavin semiquinone (dRFH$^{\cdot}$).

The nNOS oxyFMN solution was then illuminated for an appropriate period of time (~30 s) to obtain a mixture of the [Fe^{II}−CO][FMNH$^{\cdot}$] and [Fe^{II}−CO] forms of the protein. The reduced protein was subsequently flashed with 450 nm laser excitation to dissociate CO from Fe^{II}−CO and generate a transient Fe^{II} species that is able to intramolecularly transfer one electron to the FMNH$^{\cdot}$ to produce fully reduced FMN. This latter process was followed by the loss of absorbance of FMNH$^{\cdot}$ at 580−600 nm. Because the reduced protein has a strong characteristic absorption of Fe^{II}−CO at 450 nm relative to that of FMN, the 450 nm laser flash was predominately absorbed by Fe^{II}−CO. Solutions containing dRF alone in CO-degassed buffer were flashed with 450 nm laser excitation as a control, and negligible signals of much smaller magnitude were observed, as expected because of the weak absorption of dRF at 450 nm.

All of the experiments were performed at room temperature, and the sample was kept in ice between flashes. Generally, data from 20 laser flashes were averaged. Transient absorbance changes were analyzed using SIFIT, obtained from OLIS, Inc. (Jefferson, GA), and confirmed by SVD analysis on a set of traces over a range of wavelengths using Olis GlobalWorks (version 3.0).

RESULTS

Photochemical Reduction of the Oxidized nNOS oxyFMN by Deazariboflavin Semiquinone. The nNOS constructs were reduced by illumination of the proteins in the presence of dRF. The basic photochemical process by which dRFH$^{\cdot}$, which has a redox potential of −630 mV, is generated and used as the exogenous reductant to reduce redox-active proteins has been extensively described (*26*).

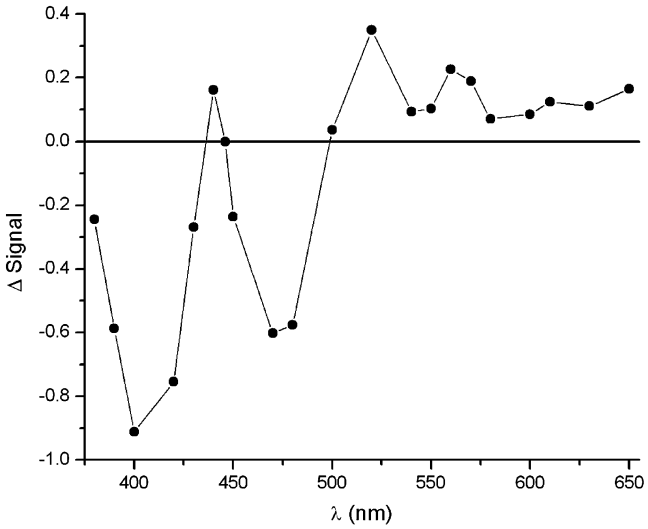

FIGURE 2: Flash-induced difference spectra of oxidized nNOS oxyFMN obtained 820 ms after a pulse of 400 nm laser excitation. Anaerobic solutions contained 7.5 μM nNOS, ~20 μM dRF, and 5 mM fresh semicarbazide in pH 7.6 buffer (40 mM Bis-Tris propane, 400 mM NaCl, 2 mM L-arginine, 1 mM Ca^{2+}, and 10% glycerol).

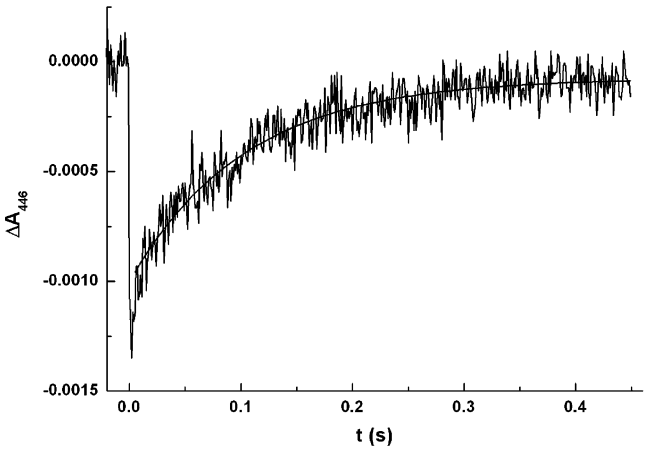

FIGURE 3: Transient trace at 446 nm obtained for oxidized nNOS oxyFMN construct after a pulse of 400 nm laser excitation. Experimental conditions were the same as in Figure 2.

A 400 nm laser-flash-induced difference spectrum of the construct in the presence of CO (Figure 2) shows that the absorption changes at 446 and 480 nm under these conditions are due to the formation of the Fe^{II}−CO complex and FMN reduction, respectively, through the reaction with dRFH$^{\cdot}$. In addition, a net positive absorbance change around 580 nm (Figure 2) indicates the formation of FMNH$^{\cdot}$. These data clearly indicate that dRFH$^{\cdot}$ can readily reduce both FMN and heme in this construct.

The reduction of FMN by dRFH$^{\cdot}$ occurs with a rate constant of ~4×10^8 M^{-1} s^{-1} (data not shown), indicating that bound FMN readily reacts with dRFH$^{\cdot}$ to generate FMNH$^{\cdot}$. The rate of the slow absorbance increase at 446 nm (Figure 3) is dependent upon the CO concentration with a second-order rate constant for CO binding to Fe^{II} having

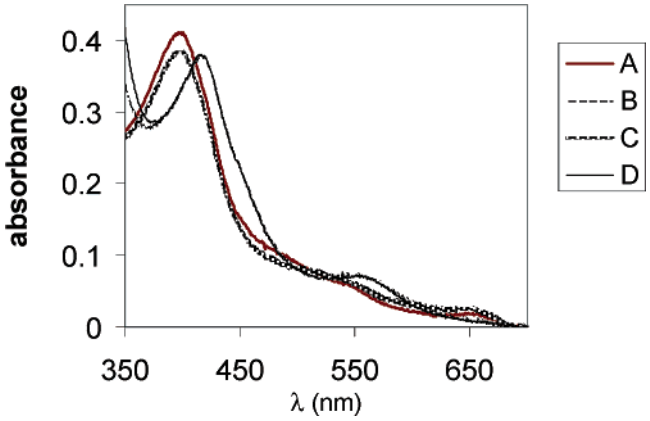

FIGURE 4: UV−vis spectra of nNOS oxyFMN construct during the oxidation/reduction cycle. Trace A, oxidized protein; trace B, reduced with dithionite solution; trace C, air oxidized showing the blue neutral $FMNH^{\cdot}$ radical; and trace D, re-reduced with a second dithionite aliquot.

a value of 2.8×10^4 M^{-1} s^{-1} (data not shown), indicating that it is due to CO binding to the Fe^{II} center of the reduced protein.

Figure 4 shows UV−vis spectra of the nNOS oxyFMN construct during the oxidation/reduction cycle. This demonstrates that, after reduction with a small volume of buffered dithionite solution, introduction of about 300 mL of air caused almost complete heme reoxidation to the high-spin ferric state. At the same time, $FMNH_2$ was rapidly oxidized to the blue neutral semiquinone $FMNH^{\cdot}$, which is very stable and is formed in very high yield, consistent with the flash-induced difference spectrum (Figure 2).

ET between the Heme and FMN Domains in the Partially Reduced nNOS oxyFMN Construct. The oxidized nNOS oxyFMN construct in the presence of dRF and CO was exposed to steady white-light illumination for various periods of time to generate the $[Fe^{II}-CO][FMNH^{\cdot}]$ form of the protein (see above). The redox potentials of the $FMN/FMNH^{\cdot}$ and $FMNH^{\cdot}/FMNH_2$ couples have been determined to be +50 and −180 mV, respectively (*23*). The apparent midpoint potential of the $Fe^{III}/Fe^{II}-CO$ couple is in the range of 0 to −50 mV under these conditions (J. C. Salerno, personal communication). Therefore, ET from $Fe^{II}-CO$ to $FMNH^{\cdot}$ is disfavored, thus allowing the formation of the $[Fe^{II}-CO]$-$[FMNH^{\cdot}]$ species in high yield.

The $[Fe^{II}-CO][FMNH^{\cdot}]$ form was then flashed by 450 nm laser excitation to dissociate CO from the $Fe^{II}-CO$ complex and form a transient Fe^{II} species. Figure 5 shows 450 nm laser-flash-induced difference spectra (upon a pulse of 450 nm laser excitation) between 400 and 480 nm for the photochemically reduced nNOS oxyFMN (Figure 5a) and nNOSoxy (Figure 5b) constructs, respectively. Note the similarities in the absorption changes at 446 and 407 nm between these two constructs, indicating the prompt release of free Fe^{II} and the subsequent slow rebinding of CO to Fe^{II}. Analyses of the traces at 450 nm for the nNOS oxyFMN construct gave the best fit with a two independent first-order model with rate constants of 10.5 ± 1 and 3.7 ± 0.5 s^{-1} (Table 1). The rate constant of the fast phase of CO rebinding (10.5 ± 1 s^{-1}) is similar to that obtained from flashing the oxidized protein in the presence of dRF and CO (10.3 ± 1.6 s^{-1}), confirming that this is due to rebinding of CO to

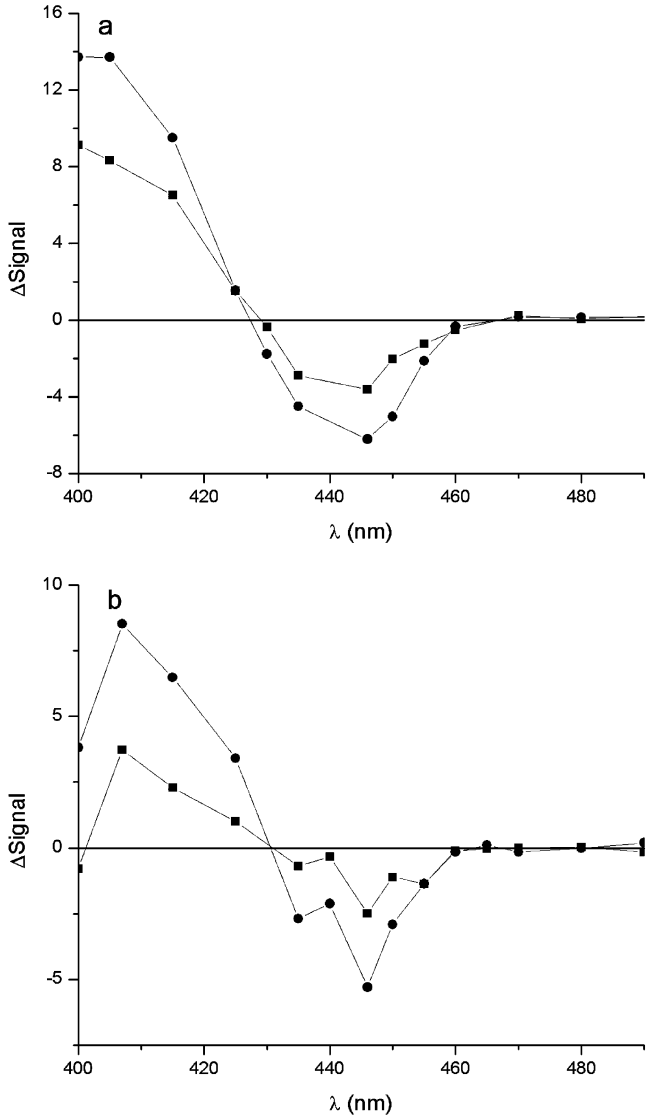

FIGURE 5: Flash-induced difference spectra (400−490 nm) of (a) reduced nNOS oxyFMN and (b) reduced nNOSoxy constructs obtained 272 ms (●) and 353 ms (■) after the 450 nm laser flash. Experimental conditions were the same as in Figure 2.

Table 1: Rate Constants of the IET (k_{et}^{obs}) and CO Rebinding (k_{CO}) of nNOS oxyFMN Either with or without Added CaM[a]

		k_{CO} (s^{-1})[b]	
	k_{et}^{obs} (s^{-1})	fast phase	slow phase
nNOS oxyFMN + CaM[c]	262 ± 40	10.5 ± 1.0 (74%)	3.7± 0.5 (26%)
nNOS oxyFMN − CaM	22 ± 2	9.5 ± 0.8 (85%)	2.2 ± 0.3 (15%)

[a] Buffer: 40 mM Bis-Tris propane, 400 mM NaCl, 2 mM L-arginine, 1 mM Ca^{2+}, and 10% glycerol at pH 7.6. dRF solutions (50 μM) with 5 mM fresh semicarbazide in the buffer were used. [b] Estimated percentage of CO rebinding in the fast or slow phase is indicated in parentheses. [c] Excess CaM added. Final [CaM] and [nNOS] are 30 and 7.5 μM, respectively.

Fe^{II}. In contrast, the kinetics of CO rebinding to Fe^{II} in the nNOSoxy construct can be best fitted by a single first-order model with a rate constant of 10.6 ± 0.4 s^{-1}. The difference in the CO-rebinding kinetics behavior between the nNOS oxyFMN and nNOSoxy constructs is related to IET between FMN and heme domains in nNOS oxyFMN (see below).

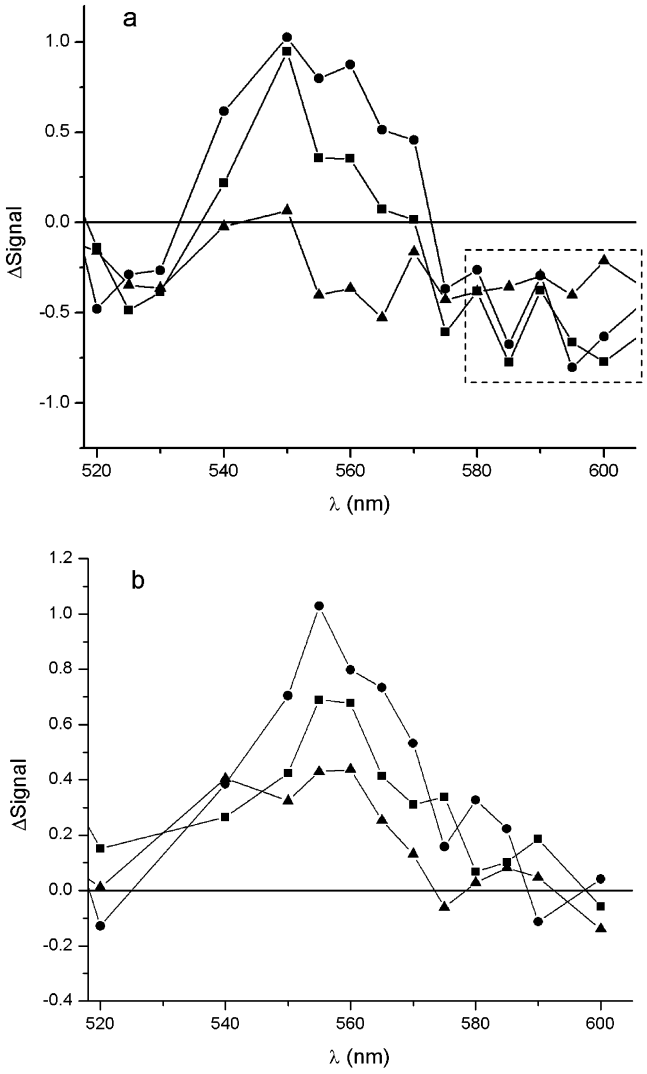

FIGURE 6: Flash-induced difference spectra (520−600 nm) of (a) reduced nNOS oxyFMN construct obtained 110 ms (●), 124 ms (■), and 374 ms (▲) and (b) reduced nNOSoxy construct obtained 138 ms (●), 150 ms (■), and 230 ms (▲) after the 450 nm laser flash. Note the region highlighted in the dashed box in a, which has a contribution from the ET between Fe^{II} and $FMNH^{\cdot}$.

CO photolysis of the [Fe^{II}−CO][$FMNH^{\cdot}$] form of nNOS oxyFMN results in a decrease of the redox potential of the Fe^{III}/Fe^{II} couple to −180 mV (J. C. Salerno, personal communication), and thereby, ET from the transient CO-free Fe^{II} (formed by the 450 nm laser) to $FMNH^{\cdot}$ may proceed. Figure 6 shows 450 nm laser-flash-induced difference spectra between 520 and 600 nm for the photochemically reduced nNOSoxy construct (which has no FMN cofactor) and the nNOS oxyFMN in the presence of CaM. Note the significant difference in the transient traces between 580 and 600 nm between the nNOS oxyFMN and nNOSoxy constructs. In particular, the absorption of nNOS oxyFMN at 600 nm rapidly decays below the baseline with a rate constant of 262 ± 40 s^{-1} (Figure 7a), followed by a slow recovery to the baseline at a longer time with a rate constant of 3.8 ± 0.3 s^{-1} (Figure 7b), similar to that of the slow phase of the CO-rebinding rate (3.1 ± 0.5 s^{-1}, see above) obtained from global analysis of the traces at 395−460 nm for nNOS oxyFMN, where Fe^{II} and Fe^{II}−CO dominate the absorption. This indicates that the biphasic behavior of CO rebinding in nNOS oxyFMN may be due to competition of CO binding

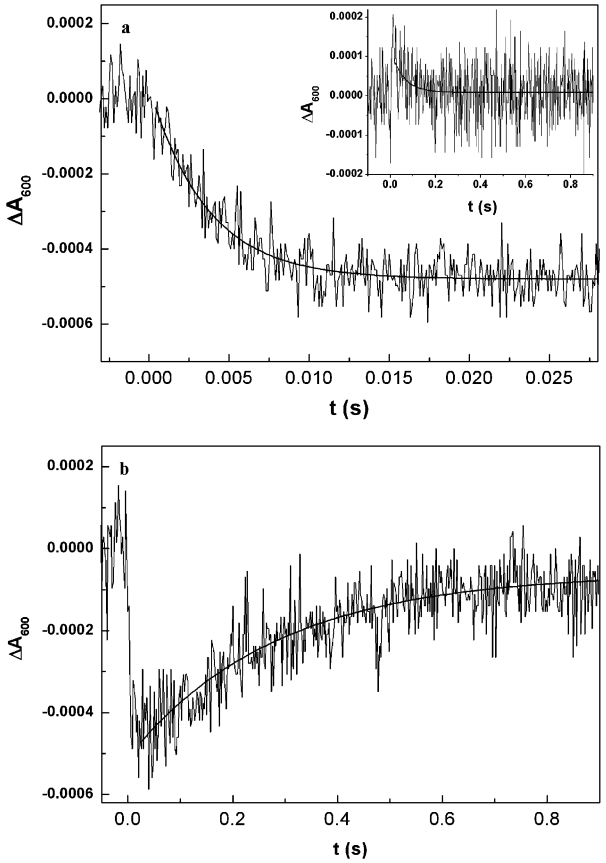

FIGURE 7: Transient trace at 600 nm at (a) shorter and (b) longer time scales obtained for the [Fe^{II}−CO][$FMNH^{\cdot}$] form of nNOS oxyFMN with added CaM flashed by the 450 nm laser. Anaerobic solutions contained 7.5 μM nNOS oxyFMN, 30 μM CaM, ~20 μM dRF, and 5 mM fresh semicarbazide in pH 7.6 buffer (40 mM Bis-Tris propane, 400 mM NaCl, 2 mM L-arginine, 1 mM Ca^{2+}, and 10% glycerol). The inset of a is of the [Fe^{II}−CO] form of the nNOSoxy construct (which does not contain FMN) flashed by the 450 nm laser under the same experimental conditions; note that the trace remains above the pre-flash baseline.

to Fe^{II} with IET between the heme and FMN domains. In contrast, the 600 nm absorption of the nNOSoxy construct stays above the baseline (Figure 6b) and decays slowly with a rate constant of 10.6 ± 0.4 s^{-1} (inset of Figure 7a). Note that $FMNH^{\cdot}$ dominates the absorption in the range of 580−600 nm. More importantly, the rate constant of the absorption change at 580−600 nm for nNOS oxyFMN is independent of the signal amplitude, i.e., the concentration of reduced protein (data not shown), indicating an intraprotein process. On the basis of these observations, we have assigned the rapid decay at 580−600 nm (Figure 7a) in the nNOS oxyFMN in the presence of CaM to the following IET process:

$$[Fe^{II}][FMNH^{\cdot}] + H^{+} \leftrightarrow [Fe^{III}][FMNH_2] \qquad (1)$$

Because Fe^{III}/Fe^{II} and $FMNH^{\cdot}/FMNH_2$ are nearly isopotential (*23*), the ET between Fe^{II} and $FMNH^{\cdot}$ is reversible and the observed rate constant is the sum of the forward (k_f) and reverse (k_r) ET steps. Thus, both k_f and k_r in nNOS oxyFMN at pH 7.6 are approximately equal to 131 ± 20 s^{-1}. The observed IET rate constant is listed in Table 1.

CO photolysis of the [Fe^{II}−CO][$FMNH^{\cdot}$] form of a murine iNOS oxyFMN construct gives a similar rapid decay at 600

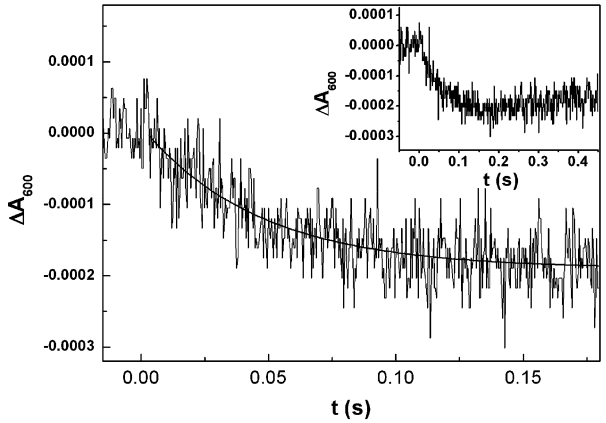

FIGURE 8: Transient trace at 600 nm for the [Fe^{II}−CO][$FMNH^{\cdot}$] form of nNOS oxyFMN without added CaM flashed by the 450 nm laser. Note that decay below the pre-flash baseline occurs on a much slower time scale than in Figure 7a. Anaerobic solutions contained 7.5 μM nNOS oxyFMN, ~20 μM dRF, and 5 mM fresh semicarbazide in pH 7.6 buffer (40 mM Bis-Tris propane, 400 mM NaCl, 2 mM L-arginine, 1 mM Ca^{2+}, and 10% glycerol). The inset shows the trace at a longer time scale; note that the trace starts to go back toward the baseline after ~0.2 s, which is due to the rebinding of CO to Fe^{II}, similar to nNOS oxyFMN with added CaM (Figure 7b).

nm with an observed rate constant of 850 ± 50 s^{-1}, which is also independent of the protein concentration (*27*). In the iNOS system, added CaM is not required because this protein binds CaM so strongly that coexpressed CaM is tightly bound during purification (*2*, *11*). This result reinforces the assignment of the absorbance change of the rat nNOS oxyFMN at 600 nm to IET between the heme and FMN domains. The difference in the rate constants between iNOS and nNOS isoforms may be due to different IET-competent conformations.

CaM Effect on the ET between the Heme and FMN Domains in the nNOS oxyFMN Construct. Figure 8 shows the transient trace at 600 nm obtained by flashing reduced nNOS oxyFMN in the absence of added CaM with 450 nm laser excitation. Note the remarkable difference in the time scale for the decay phase between nNOS oxyFMN incubated with added CaM (Figure 7a) and that in the absence of added CaM (Figure 8). The rate constant for nNOS oxyFMN without added CaM is 22 ± 2 s^{-1}, which is approximately a 10-fold decrease compared to that with added CaM (Table 1). Note that the rate constant is also independent of the signal amplitude (data not shown), consistent with an intraprotein ET process (eq 1). Scheme 1 summarizes the processes that take place after photolysis of the Fe^{II}−CO complex in the reduced nNOS oxyFMN construct. Although the nNOS oxyFMN protein was purified in the presence of CaM, this cofactor is relatively weakly bound, and thus, during the purification, all of the CaM may be lost. We believe that the slow but still substantial rate of IET in the absence of CaM is real and may reflect the different conformations of the CaM-bound and CaM-free proteins.

CaM Effect on EPR Spectra of High-Spin Heme in the nNOS oxyFMN Construct. Figure 9 shows the effect of CaM on the g_{max} peak of the EPR spectrum of the nNOS oxyFMN high-spin ferriheme. The central peak (—) is the g_{max} signal from nNOSoxy containing bound arginine and H_4B; g_{max} ~ 7.72. The dashed trace shows the corresponding feature from nNOS oxyFMN in the absence of CaM; the peak position is

Scheme 1: Summary of Processes Occurring upon CO Photolysis[a]

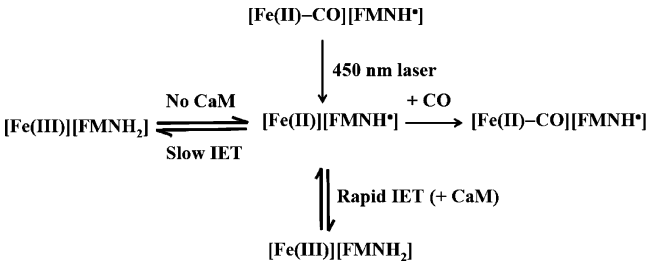

[a] Starting from the Fe^{II}−CO complex, laser flash photolytic dissociation of CO results in a drop of the heme redox potential and ET from Fe^{II} to $FMNH^{\cdot}$ proceeds with a rate constant of 22 s^{-1} (without added CaM) or 260 s^{-1} (with added CaM). Subsequently, in the absence of added CaM, CO rebinding to Fe^{II} competes with the IET between the heme and FMN domains, whereas in the presence of CaM, CO rebinding is a poor competitor for IET and CO binds only to a fraction of the reduced heme. A CO/Ar mixture was used to slow CO rebinding and favor IET from Fe^{II} to $FMNH^{\cdot}$, making the loss of $FMNH^{\cdot}$ observable as a bleach between 580 and 600 nm.

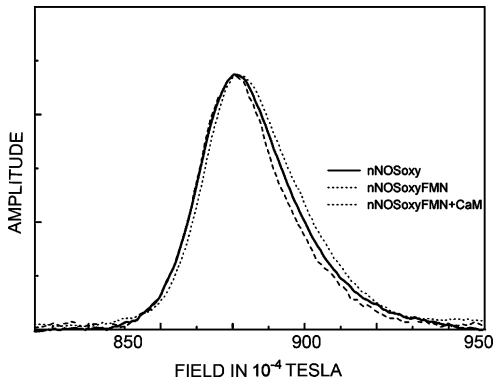

FIGURE 9: EPR spectra of high-spin ferriheme, showing the effects of CaM binding to the nNOS oxyFMN construct (adapted from ref 23). (—) nNOSoxy, (- - -) nNOS oxyFMN construct without added CaM, and (•••) nNOS oxyFMN construct with Ca^{2+} and CaM (nNOS oxyFMN + CaM). All samples contained approximately 45 μM heme. The amplitude of the upper left trace for nNOS oxyFMN was slightly decreased to facilitate the comparison of line shapes. Instrument settings were microwave power, 2 mW; modulation amplitude, 10 G; modulation frequency, 100 kHz; microwave frequency, 9.51 GHz; and temperature, 15 K.

only slightly shifted to a high field relative to the oxygenase construct, but the high-field edge of the line is noticeably shifted to a lower field. The dotted trace shows the g_{max} signal from nNOS oxyFMN in the presence of Ca^{2+} and CaM; note that g_{max} shifts to $g \sim 7.69$ and the line is significantly broader. We attribute these effects to CaM-induced association of the FMN-binding domain. High-spin ferrihemes are well-described by the $S = {}^5/_2$ spin Hamiltonian $D\{Sz^2 - 1/3[S(S+1)]\} + E(Sx^2 - Sy^2)$, where the zero-field splitting parameters E and D reflect a differential admixture of low-lying states into the ground state $^6A_1$ sextet by spin−orbit coupling because of tetragonal and rhombic splitting of the t_{2g} 3d orbitals (*25*). For a large D, the primary effect of increases in E/D is to split g_x and g_y about the axial value of 6; second-order effects decrease g_z and $(g_x + g_y)/2$. The asymmetric lines in Figure 9 are produced by distributions of E/D centered on 0.083. The sharp high-field side of the lines reflects a weaker dependence of the field position as E/D increases.

DISCUSSION

The previous crystal structures and functional studies (*8*−*10*) primarily concerned an enzyme conformation, which serves as the input state for reduction of FMN by electrons from NADPH and FAD in the reductase domain but not for the subsequent IET from FMN to heme in the oxygenase domain. The putative output state is envisioned as a complex between oxygenase and FMN-binding domains. We have for the first time described the design and production of a novel two-domain oxyFMN construct of rat nNOS to allow for the formation of the output state from FMN to the oxygenase domain (*23*). The homologous dimeric oxyFMN construct is active and stable, binds cofactors nearly stoichiometrically, and has characteristic absorption and EPR spectra similar to the holoenzyme (*23*). Potentiometric titration studies have shown that the redox potentials of the oxyFMN construct are comparable to the holoenzyme (*23*). Therefore, the truncated construct appears to be a reasonable approximation of the holoenzyme. We expect the output state of oxyFMN constructs to be a good model for the output state of the holoenzyme. The experiments reported here were designed to measure heme−FMN ET rates in the output state and to investigate the possibility of CaM dependence outside the reductase complex.

The slow phase of CO rebinding in nNOS oxyFMN (Table 1) could be due to the fraction of the heme competent to bind CO (i.e., Fe^{II}). In nNOS oxyFMN with added CaM, because the IET equilibrium (eq 1) is fast compared to CO rebinding, a 3-fold slower CO-rebinding rate relative to that of the oxygenase construct could be due to only one-third of the heme being reduced. This places the potential of the second FMN couple (i.e., $FMNH^{\cdot}/FMNH_2$) ~18 mV higher than the heme couple, consistent with the reported potentials (*23*).

Previous studies on heme reduction in NOS isoforms from CO-binding kinetics gave rate constants of 3−4 and 0.9−1.5 s^{-1} for nNOS and iNOS holoenzymes (*12*, *28*, *29*), respectively. In this work, we have used laser flash photolysis of CO dissociation in comparative studies on the partially reduced nNOS oxyFMN construct (i.e., $[Fe^{II}-CO][FMNH^{\cdot}]$) and the reduced single-domain heme oxygenase construct (i.e., $[Fe^{II}-CO]$) to directly determine the kinetics of IET between the FMN and heme domains in the oxyFMN construct. Because the experiments reported here do not involve any step other than the IET between the FMN and heme domains, they provide *direct* determination of the kinetics of this process. The present study demonstrates that the observed slow rates of heme reduction in NOS holoenzymes by CO-binding kinetics (*12*, *28*, *29*) are probably the rates of CO binding to Fe^{II}.

It is important to note that, however, the kinetics reported here are "output-state" kinetics and, hence, may not be expected to correspond directly to the kinetics of ET in the holoenzyme, in which FMN has to undergo dissociation from the input-state complex and reassociation with the oxygenase domain before rapid ET can occur (Figure 1). It is possible that the presence of the two-domain "dehydrogenase" unit would affect the orientation of the FMN and oxygenase domains in the output state of the holoenzyme enough to produce a slower rate. Thus, the actual rate of the IET in the holoenzyme will likely fall between that of the two-domain construct (an "output" state model) and the lower value determined from CO-binding kinetics. A comparative study of the IET in the holoenzyme is underway and will show if the remarkable difference with the previously reported IET rates by CO-binding kinetics is due to the different methodology or the different protein constructs.

Scheme 2: Proposed Mechanism of Interdomain IET between the FMN and the Heme Domains in the oxyFMN Construct, Activated by CaM Binding[a]

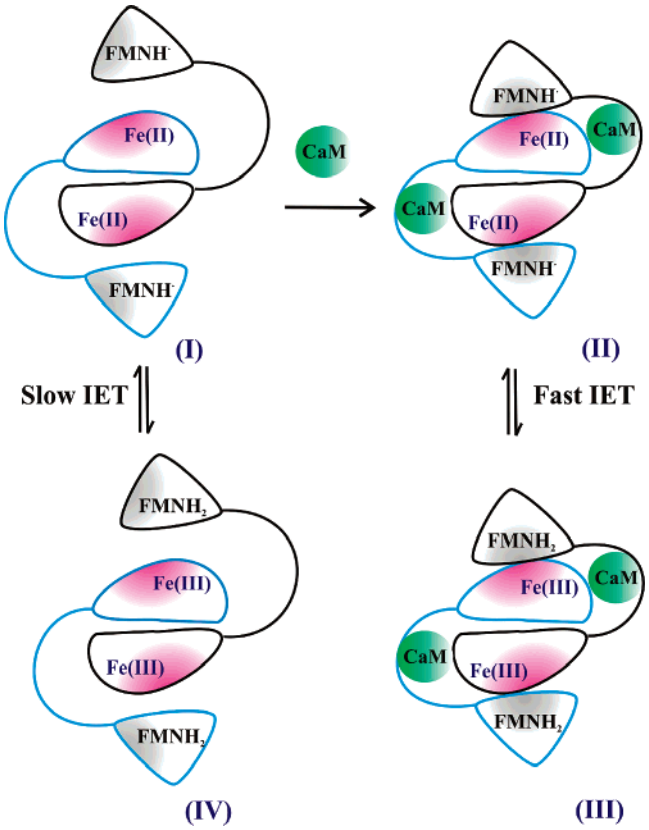

[a] The two subunits are shown in black and blue, respectively. Note that the fast IET is triggered by the large structural rearrangement upon CaM binding.

The IET rates in the nNOS oxyFMN construct were increased nearly 10-fold upon adding CaM. Note that CaM has a minimal effect on the thermodynamics of redox processes in the construct (*23*), similar to the holoenzyme (*20*). Thus, this work provides the first direct evidence of CaM control of ET between the FMN and heme domains through facilitation of FMN/heme interactions in the output state (i.e., a *dynamic* factor). A structural interpretation of this mechanism (Scheme 2) is as follows. In the absence of CaM, Fe^{II} is far away from the $FMNH^{\cdot}$ (structure I), thereby being unable to rapidly transfer one electron to $FMNH^{\cdot}$ and reduce it to $FMNH_2$. Upon adding CaM, a large-scale motion brings the heme and FMN domains closer to one another (putative output state, structure II), thereby facilitating fast IET between these two domains. Therefore, CaM controls IET between the heme and FMN domains by a conformational gated mechanism.

The effect of CaM binding on interdomain interactions is further manifested in the EPR spectra (Figure 9), in which the asymmetry of the peak is due to the details of strain broadening by the distribution of *E*/*D*. We have presented evidence in a separate paper for effects of CaM on the heme

environment in oxyFMN constructs and magnetic interactions between FMN semiquinone and ferriheme in a murine iNOS oxyFMN (*23*). The probable cause of the observed distortions of the heme environment upon adding CaM is the CaM-dependent interaction of the surface-charge distributions adjacent to the heme group. These effects have not been reported in the holoenzyme, probably because most of the holoenzyme is in the input state.

Previously, CaM control of NOS ET was widely believed to be localized within the reductase portion of the enzyme (*30*, *31*). Evidence for multiple steps of CaM control was attributed to separate CaM modulation of FMN and heme reductions (*32*, *33*). Other workers have convincingly argued that FAD/FMN ET per se is not CaM-controlled and that access of FMN to external electron acceptors is coupled to CaM activation and pyridine nucleotide binding (*34*). Recently, a study on CaM mutants suggests that the primary control of ET in eNOS and nNOS is through CaM activation of the release of the FMN-binding domain from the reductase complex input state, making FMN accessible to exogenous acceptors such as cytochrome *c* (*35*). The requirement of CaM for iNOS, in contrast, is apparently associated with alignment of FMN and heme (*2*, *11*, *35*, *36*). Recently, we showed that CaM-free iNOS constitutively reduces cytochrome *c* and that iNOS requires only the two N-terminal EF hands of CaM for NO synthesis (*36*).

The work presented here establishes a role for CaM in the formation of the nNOS output state. This may be the original role of CaM in the evolution of NOSs and could predate the evolution of the modern control elements. It will be of interest to ascertain whether the effects of these control elements are limited to input-state stabilization, or if they also affect output-state formation.

There are numerous biological ET systems whose function depends upon recognition, optimal orientation, and proper interaction between proteins that shuttle electrons (*37*−*41*). Electrostatic interactions between protein surfaces are important in molecular recognition, making the distribution of charged surface residues an active determinant of ET kinetics in redox proteins. The effect of such interactions on protein ET is an intense area of current interest (*42*, *43*). Interestingly, the recent reported structure of the nNOS reductase supports plausible domain movements triggered by CaM binding, which may be primarily driven by electrostatic interactions between the charged surface residues on the heme and FMN domains (*8*). Further, laser flash photolysis studies on mutants of residues related to the possible docking between the FMN and heme domains will provide additional insights into the role of the surface charge in the coupling of IET and NO synthesis in this important enzyme.

It is now obvious that electron-shuttle mechanisms are a common alternative to solid-state electron-tunneling pathways. Biological redox systems with internal conformational shuttles are molecular-scale electromechanical devices and present the potential for functioning as molecular-scale switches. In the case of NOS, we have an example of a biosensor (i.e., CaM) activated electrical switch.

In conclusion, laser flash photolysis of an [Fe^{II}−CO]-[$FMNH^{\cdot}$] form of the novel nNOS oxyFMN construct has allowed us to directly observe the discrete IET step between FMN and heme in nNOS. This work also provides the first direct evidence of CaM in controlling ET between FMN and heme domains in nNOS and the production of the nNOS output state in NO formation.

REFERENCES

1. Schmidt, H. H. H. W., and Walter, U. (1994) NO at work, *Cell 78*, 919−925.
2. Alderton, W. K., Cooper, C. E., and Knowles, R. G. (2001) Nitric oxide synthases: Structure, function and inhibition, *Biochem. J. 357*, 593−615.
3. Wei, C. C., Crane, B. R., and Stuehr, D. J. (2003) Tetrahydrobiopterin radical enzymology, *Chem. Rev. 103*, 2365−2383.
4. Fedorov, R., Vasan, R., Ghosh, D. K., and Schlichting, I. (2004) Structures of nitric oxide synthase isoforms complexed with the inhibitor AR-R17477 suggest a rational basis for specificity and inhibitor design, *Proc. Natl. Acad. Sci. U.S.A. 101*, 5892−5897.
5. Crane, B. R., Arvai, A. S., Ghosh, D. K., Wu, C., Getzoff, E. D., Stuehr, D. J., and Tainer J. A. (1998) Structure of nitric oxide synthase oxygenase dimer with pterin and substrate, *Science 279*, 2121−2126.
6. Raman, C. S., Li, H., Martasek, P., Kral, V., Masters, B. S. S., and Poulos, T. L. (1998) Crystal structure of constitutive endothelial nitric oxide synthase: A paradigm for pterin function involving a novel metal center, *Cell 95*, 939−950.
7. Fedorov, R., Hartmann, E., Ghosh, D. K., and Schlichting, I. (2003) Crystal structures of cyanide complexes of P450cam and the oxygenase domain of inducible nitric oxide synthase—Structural models of the short-lived oxygen complexes, *J. Biol. Chem. 278*, 45818−45825.
8. Garcin, E. D., Bruns, C. M., Lloyd, S. J., Hosfield, D. J., Tiso, M., Gachhui, R., Stuehr, D. J., Tainer, J. A., and Getzoff, E. D. (2004) Structural basis for isozyme-specific regulation of electron transfer in nitric oxide synthase *J. Biol. Chem. 279*, 37918−37927.
9. Zhang, J., Martásek, P., Paschke, R., Shea, T., Masters, B. S. S., and Kim, J. J. P. (2001) Crystal structure of the FAD/NADPH-binding domain of rat neuronal nitric-oxide synthase—Comparisons with NADPH-cytochrome P450 oxidoreductase, *J. Biol. Chem. 276*, 37506−37513.
10. Wang, M., Roberts, D. L., Paschke, R., Shea, T. M., Masters, B. S. S., and Kim, J. J. (1997) Three-dimensional structure of NADPH-cytochrome P450 reductase: Prototype for FMN- and FAD-containing enzymes, *Proc. Natl. Acad. Sci. U.S.A. 94*, 8411−8416.
11. Roman, L. J., Martásek, P., and Masters, B. S. S. (2002) Intrinsic and extrinsic modulation of nitric oxide synthase activity, *Chem. Rev. 102*, 1179−1190.
12. Panda, K., Ghosh, S., and Stuehr, D. J. (2001) Calmodulin activates intersubunit electron transfer in the neuronal nitric-oxide synthase dimer, *J. Biol. Chem. 276*, 23349−23356.
13. Zemojtel, T., Scheele, J. S., Martásek, P., Masters, B. S. S., Sharma, V. S., and Magde, D. (2003) Role of the interdomain linker probed by kinetics of CO ligation to an endothelial nitric oxide synthase mutant lacking the calmodulin binding peptide (residues 503−517 in bovine), *Biochemistry 42*, 6500−6506.
14. Gribovskaja, I.; Brownlow, K. C.; Dennis, S. J.; Rosko, A. J.; Marletta, M. A.; Stevens-Truss, R. (2005) Calcium-binding sites of calmodulin and electron transfer by inducible nitric oxide synthase, *Biochemistry 44*, 7593−7601.
15. Salerno, J. C., Harris, D. E., Irizarry, K., Patel, B., Morales, A. J., Smith, S. M., Martásek, P., Roman, L. J., Masters, B. S. S., Jones, C. L., Weissman, B. A., Lane, P., Liu, Q., and Gross, S. S. (1997) An autoinhibitory control element defines calcium-regulated isoforms of nitric oxide synthase, *J. Biol. Chem. 272*, 29769−29777.
16. Jáchymová, M., Martásek, P., Panda, S., Roman, L. J., Panda, M., Shea, T. M., Ishimura, Y., Kim, J.-J. P., and Masters, B. S. S. (2005) Recruitment of governing elements for electron transfer in the nitric oxide synthase family, *Proc. Natl. Acad. Sci. U.S.A. 102*, 15833−15838.
17. Sagami, I., Sato, Y., Noguchi, T., Miyajima, M., Rozhkova, E., Daff, S., and Shimizu, T. (2002) Electron transfer in nitric-oxide synthase, *Coord. Chem. Rev. 226*, 179−186.
18. Udit, A. K., Belliston-Bittner, W., Glazer, E. C., Nguyen, Y. H. L., Gillan, J. M., Hill, M. G., Marletta, M. A., Goodin, D. B., and Gray, H. B. (2005) Redox couples of inducible nitric oxide synthase, *J. Am. Chem. Soc. 127*, 11212−11213.
19. Bayachou, M., and Boutros, J. A. (2004) Direct electron transfer to the oxygenase domain of neuronal nitric oxide synthase

(NOS): Exploring unique redox properties of NOS enzymes, *J. Am. Chem. Soc. 126*, 12722−12723.
20. Gao, Y. T., Smith, S. M. E., Wenberg, J. B., Montgomery, H. J., Newman, E., Guillemette, J. G., Ghosh, D. K., Roman, L. J., Martasek, P., and Salerno, J. C. (2004) Thermodynamics of oxidation−reduction reactions in mammalian nitric oxide synthase isoforms, *J. Biol. Chem. 279*, 18759−18766.
21. Guan, Z., and Iyanagi, T. (2003) Electron transfer is activated by calmodulin in the flavin domain of human neuronal nitric oxide synthase, *Arch. Biochem. Biophys. 412*, 65−76.
22. Ghosh, D. K., and Salerno J. C. (2003) Nitric oxide synthases: Domain structure and alignment in enzyme function and control, *Front. Biosci. 8*, 193−209.
23. Ghosh, D. K., Holliday, M. A., Thomas, C., Weinberg, J. B., Smith, S. M. E., and Salerno, J. C. (2006) Towards a NOS output state: Design and properties of NOS oxygenase/FMN domain constructs, *J. Biol. Chem. 281*, 14173−14183.
24. Ghosh, D. K., Wu, C., Pitters, E., Moloney, M., Werner, E. R., Mayer, B., and Stuehr, D. J. (1997) Characterization of the inducible nitric oxide synthase oxygenase domain identifies a 49 amino acid segment required for subunit dimerization and tetrahydrobiopterin interaction, *Biochemistry 36*, 10609−10619.
25. Salerno, J. C., McMillan, K., and Masters, B. S. S. (1996) Binding of intermediate, product, and substrate analogs to neuronal nitric oxide synthase. Ferriheme is sensitive to ligand-specific effects in the L-arginine binding site, *Biochemistry 35*, 11839−11845.
26. Tollin, G. (2001) Interprotein and intraprotein electron-transfer mechanisms, In *Electron Transfer in Chemistry* (Balzani, V., Ed.) Vol. 4, pp 202−231, Wiley-VCH, Weinheim, Germany.
27. Feng, C., Thomas, C., Holliday, M. A., Tollin, G., Salerno, J. C., Ghosh, D. K., and Enemark, J. H. (2006) Direct measurement by laser flash photolysis of intramolecular electron transfer in a two-domain construct of murine inducible nitric oxide synthase, *J. Am. Chem. Soc. 128*, 3808−3811.
28. Adak, S., Curran, C. M. L., and Stuehr, D. J. (2001) Chimeras of nitric-oxide synthase types I and III establish fundamental correlates between heme reduction, heme−NO complex formation, and catalytic activity, *J. Biol. Chem. 276*, 23246−23252.
29. Santolini, J., Meade, A. L., and Stuehr, D. J. (2001) Differences in three kinetic parameters underpin the unique catalytic profiles of nitric-oxide synthases I, II, and III, *J. Biol. Chem. 276*, 48887−48898.
30. Gachhui, R., Presta, A., Bentley, D. F., Abu-Soud, H. M., McArthur, R., Brudvig, G., Ghosh, D. K., Stuehr, D. K. (1996) Characterization of the reductase domain of rat neuronal nitric oxide synthase generated in the methylotrophic yeast *Pichia pastoris*−Calmodulin response is complete within the reductase domain itself, *J. Biol. Chem. 271*, 20594−20602.
31. Sheta, S., McMillan, K., and Masters, B. S. S. (1994) Evidence for a bidomain structure of constitutive cerebellar nitric oxide synthase *J. Biol. Chem. 269*, 15147−15153.
32. Abu-Soud, H. M., Yoho, Y. L., and Stuehr, D. J. (1994) Calmodulin controls neuronal nitric oxide synthase by a dual mechanism−Activation of intradomain and interdomain electron transfer, *J. Biol. Chem. 269*, 32047−32050.
33. Matsuda, H., and Iyanagi, T. (1999) Calmodulin activates intramolecular electron transfer between the two flavins of neuronal nitric oxide synthase flavin domain, *Biochim. Biophys. Acta 1473*, 345−355.
34. Craig, D. H., Chapman, S. K., and Daff, S. (2002) Calmodulin activates electron transfer through neuronal nitric-oxide synthase reductase domain by releasing an NADPH-dependent conformational lock, *J. Biol. Chem. 277*, 33987−33994.
35. Newman, E., Spratt, D. E., Mosher, J., Cheyne, B., Montgomery, H. J., Wilson, D. L., Weinberg, J. B., Smith, S. M., Salerno, J. C., Ghosh, D. K., and Guillemette, J. G. (2004) Differential activation of nitric-oxide synthase isozymes by calmodulin-troponin C chimeras, *J. Biol. Chem. 279*, 33547−33557.
36. Spratt, D. E., Newman, E., Mosher, J., Ghosh, D. K., Salerno, J. C., and Guillemette, J. G. (2006) Activation of nitric oxide synthase isozymes by calmodulin EF hand pairs, *FEBS Lett.*, in press.
37. Leys, D., and Scrutton, N. S. (2005) Electrical circuitry in biology: Emerging principles from protein structure, *Curr. Opin. Struct. Biol. 14*, 642−647.
38. Hoffman, B. M., Celis, L. M., Cull, D. A., Patel, A. D., Seifert, J. L., Wheeler, K. E., Wang, J. Y., Yao, J., Kurnikov, I. V., and Nocek, J. M. (2005) Differential influence of dynamic processes on forward and reverse electron transfer across a protein−protein interface, *Proc. Natl. Acad. Sci. U.S.A. 102*, 3564−3569.
39. Patel, A. D., Nocek, J. M., and Hoffman, B. M. (2005) Equilibrium/nonequilibrium initial configurations in forward/reverse electron transfer within mixed-metal hemoglobin hybrids, *J. Am. Chem. Soc. 127*, 16766−16767.
40. Liang, Z. X., Kurnikov, I. V., Nocek, J. M., Mauk, A. G., Beratan, D. N., and Hoffman, B. M. (2004) Dynamic docking and electron transfer between Zn-myoglobin and cytochrome b_5, *J. Am. Chem. Soc. 126*, 2785−2798.
41. Feng, C., Kedia, R. V., Hazzard, J. T., Hurley, J. K., Tollin, G., and Enemark, J. H. (2002) Effect of solution viscosity on intramolecular electron transfer in sulfite oxidase, *Biochemistry 41*, 5816−5821.
42. Hurley, J. K., Morales, R., Martinez-Julvez, M., Brodie, T. B., Medina, M., Gomez-Moreno, C., and Tollin, G. (2002) Structure−function relationships in *Anabaena* ferredoxin/ferredoxin:$NADP^+$ reductase electron transfer: Insights from site-directed mutagenesis, transient absorption spectroscopy and X-ray crystallography, *Biochim. Biophys. Acta 1554*, 5−21.
43. Feng, C., Wilson, H. L., Hurley, J. K., Hazzard, J. T., Tollin, G., Rajagopalan, K. V., and Enemark, J. H. (2003) Essential role of conserved arginine 160 in intramolecular electron transfer in human sulfite oxidase, *Biochemistry 42*, 12235−12242.

BI060223N